Carlo Gorla[1]
Mem. ASME, Mem. AGMA
e-mail: carlo.gorla@polimi.it

Piermaria Davoli
e-mail: piermaria.davoli@polimi.it

Francesco Rosa
e-mail: francesco.rosa@polimi.it

Claudio Longoni
e-mail: claudio.longoni@mecc.polimi.it

Dipartimento di Meccanica,
Politecnico di Milano,
I-20156 Milano, Italy

Franco Chiozzi
e-mail: franco.chiozzi@bettinelli.it

Alessandro Samarani
e-mail: alessandro.samarani@bettinelli.it

CDS-Bettinelli F.Lli SPA,
I-26010 Bagnolo Cremasco (CR), Italy

Theoretical and Experimental Analysis of a Cycloidal Speed Reducer

In this paper, a theoretical and experimental investigation on an innovative cycloidal speed reducer is presented. The typical cycloid drive has a planet wheel, the profile of which is the internal offset of an epitrochoid meshing with cylindrical rollers connected to the case. This reducer, on the contrary, has an external ring gear, the transverse profile of which is the external offset of an epitrochoid and engages with the planet wheel by means of cylindrical rollers. This paper investigates the structural characteristics and the kinematic principles of this type of reducer. A theoretical approach based on the theory of gearing (following Litvin's approach) is developed and compared to a development of Blanche and Yang's approach. Furthermore, a simplified procedure to calculate the force distribution on cycloid drive elements, its power losses, and theoretical mechanical efficiency is presented. The effects of design parameters on the values of forces are studied for an optimal design of this type of reducer. The theoretical model is tuned on the basis of the results of tests made on purpose. The mechanical efficiency dependency on speed and torque is described. The main aim of this work is to tune a theoretical model in order to predict the operating behavior of the cycloid drive and to improve its design procedure. [DOI: 10.1115/1.2978342]

1 Introduction

The cycloidal speed reducers, or cycloid drives, are a family of reduction gear mechanisms designed for precise motion control. As shown in Fig. 1, the components of a typical cycloid drive are an input shaft with a crank, a planet wheel meshing with cylindrical rollers mounted on an external ring, and an output shaft with cylindrical pins engaging with planet wheel holes. The profile of the planet gear is a curve derived from an epitrochoid, a curve of the family of cycloids. Cycloid drives rely on an eccentric motion to convert the rotation of the input shaft into a wobbly cycloidal motion of the planet wheel; this motion is then converted back into a rotation of the output shaft (concentric to the input shaft) by means of some cylindrical pins fixed on the output shaft, and, in this way, the speed reduction is accomplished.

Much research on cycloid drives is present in literature. Some is mainly focused on the operating principles, the methods for the generation of the profile of the planet wheel and the analytical calculation of the forces. Litvin and Feng [1] developed a general method for the generation and design of cycloid drives, deriving the equations of cycloidal curves in parametric form, by applying the theory of gearing. Malhotra and Parameswaran [2] presented a procedure to calculate the forces on the cycloid speed reducer elements, as well as the theoretical efficiency, showing the influence of the different design parameters.

More recent works mainly deal with the optimization of these reducers or propose some new configurations, with respect to the traditional one. In order to increase the efficiency of this type of reducer, Blanche and Yang [3] developed an analytical model of the cycloid drive, using complex vectors, to investigate the effects of machining tolerances on backlash and torque ripples. Chmurawa and Lokiec [4] proposed a modification of the profile of the planet wheel. Yan and Lai [5] applied the theory of envelope to derive the surface equation of a ring gear of an elementary planetary gear train, the planet wheel of which having cylindrical teeth. Hwang and Hsieh [6] determined a feasible design region without undercutting on the tooth profile or interference between the adjacent pins.

In this paper the cycloid drive shown in Fig. 2 is studied. This mechanism is composed of an input shaft with a crank, a planet wheel, a ring gear, and an output shaft with cylindrical pins, but the cylindrical rollers are mounted on the planet wheel and mesh with the inner profile of the external ring gear.

The most common way of studying the traditional mechanism is based on the consideration that the motion of the cylindrical roller is identical to the motion of a circle of radius R_r rigidly connected to a generating circle of radius R_g that rolls without slipping on a base circle of radius R_b (Fig. 3). It is worth noting that the ratio R_b/R_g must be an integer, otherwise the inner profile of the ring gear would not form a closed loop. If there is one cylindrical roller more than the lobes ($n=m+1$) on the inner surface of the ring gear profile, the new cyclo-drive has a reduction ratio equal to $\tau=(n-m)/n=1/n$; on the contrary the traditional reducer has a reduction ratio equal to $\tau=(n-m)/m=1/(n-1)$ (see Ref. [3]). The proposed solution can then provide a greater reduction ratio with about the same dimensions of the traditional one. Another peculiarity of this reducer is that the output and input shafts have the same direction of rotation. As a consequence, there is a reduction of the relative speed between the races of the bearing between the crank on the input shaft and the planet wheel, which could have a positive effect on the power loss. These are the main reasons for our interest in this geometric configuration. The last, but not least, reason is the use of a wire Electro Discharge Machining (EDM) machine to manufacture the profile: Some experimental tests on this wire EDM machine showed a greater accuracy in manufacturing internal profiles than external.

The profile of the ring gear is derived by applying the theory of gearing. Then, a simplified procedure to calculate the distribution

[1]Corresponding author.

Contributed by the Power Transmission and Gearing Committee of ASME for publication in the JOURNAL OF MECHANICAL DESIGN. Manuscript received July 31, 2007; final manuscript received May 27, 2007; published online September 30, 2008. Review conducted by Avinash Singh. Paper presented at the ASME 2007 Design Engineering Technical Conferences and Computers and Information in Engineering Conference (DETC2007), Las Vegas, NV, September 4–7, 2007.

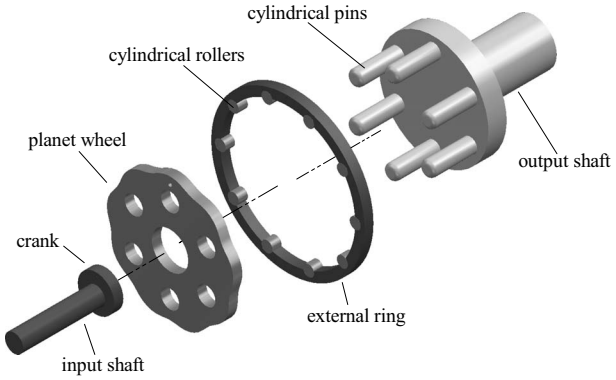

Fig. 1 Typical structure of a cycloidal speed reducer

of forces on the elements of this kind of cycloid drive, its power loss and theoretical mechanical efficiency, is presented. Furthermore, the results of some experimental tests are illustrated and discussed.

2 Generation of the Ring Gear Profile

In the following, even if the actual mechanism is three dimensional, it is studied as a planar problem, since all the planar sections normal to the axis are identical. Then we speak about surfaces, even if we study and write equations of planar curves, since the surfaces can be easily obtained by extruding the curves perpendicularly to their plane.

The correct meshing between the cylindrical rollers and the inner surface of the ring gear requires that these two surfaces are

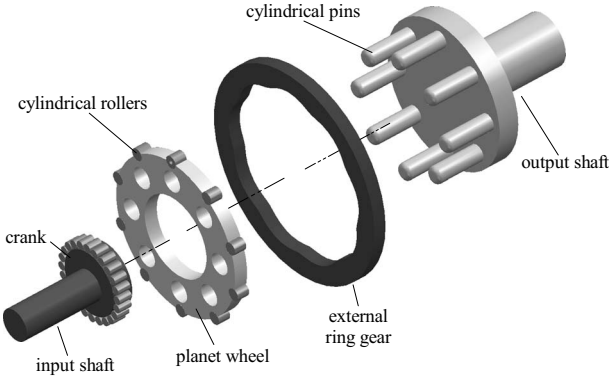

Fig. 2 Exploded view of a cycloidal speed reducer with an external ring gear and cylindrical rollers mounted on the planet wheel

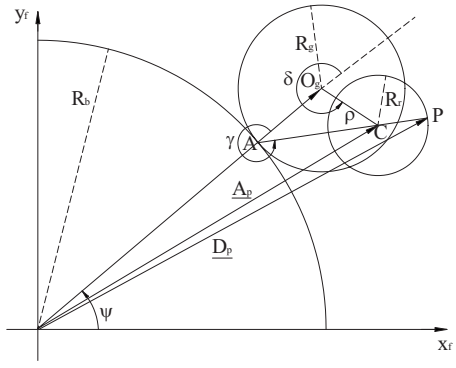

Fig. 3 Location of the contact point *P* between the roller and ring gear

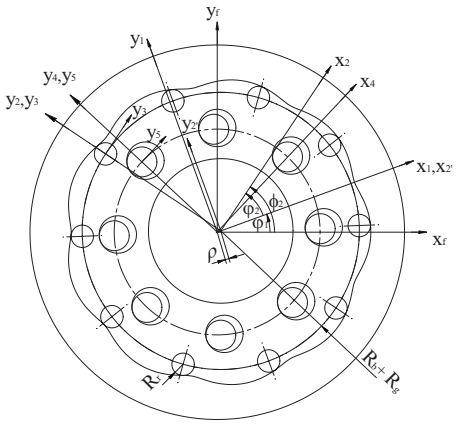

Fig. 4 Reference frames utilized for the generation of the ring gear profile

conjugated. This requirement can be fulfilled if the inner surface of the ring gear is the envelope of the family of surfaces of the cylindrical rollers during their motion. Practically, the desired motion is imposed on the input shaft, crank, and planet wheel; subsequently, the family of surfaces of the cylindrical rollers is obtained. Finally, the envelope (that is the equation of the inner ring gear surface) of the family itself is derived. The theory of gearing (see Refs. [7,8,1]) is applied to accomplish these calculations, since it does not require any preliminary assumption or simplification about the resulting ring gear inner profile.

As a first step, in order to describe the relative motions, a set of reference frames has been conceived (see Fig. 4): $\mathbf{S}_f$, which is rigidly connected to the case; $\mathbf{S}_1$, which is rigidly connected to the input shaft; $\mathbf{S}_{2'}$, which is rigidly connected to the input shaft, but eccentric with respect to $\mathbf{S}_1$; $\mathbf{S}_2$, which is rigidly connected to the planet wheel; $\mathbf{S}_3$, which is rigidly connected to the planet wheel and the origin coincident with the center of a generic roller; $\mathbf{S}_4$, which is rigidly connected to the output shaft; and $\mathbf{S}_5$, which is rigidly connected to the output shaft and the origin coincident with the center of a generic pin.

The following transformation matrices among the reference frames describe the sought motion of this mechanism:

$$\mathbf{M}_{f,1}(\varphi_1) = \begin{bmatrix} \cos\varphi_1 & \sin\varphi_1 & 0 \\ -\sin\varphi_1 & \cos\varphi_1 & 0 \\ 0 & 0 & 1 \end{bmatrix} \tag{1}$$

$$\mathbf{M}_{1,2'} = \begin{bmatrix} 1 & 0 & \rho \\ 0 & 1 & 0 \\ 0 & 0 & 1 \end{bmatrix} \tag{2}$$

$$\mathbf{M}_{2',2}(\varphi_2) = \begin{bmatrix} \cos\varphi_2 & \sin\varphi_2 & 0 \\ -\sin\varphi_2 & \cos\varphi_2 & 0 \\ 0 & 0 & 1 \end{bmatrix} \tag{3}$$

$$\mathbf{M}_{2,3} = \begin{bmatrix} 1 & 0 & 0 \\ 0 & 1 & R_b + R_g \\ 0 & 0 & 1 \end{bmatrix} \tag{4}$$

$$\mathbf{M}_{f,3}(\varphi_1, \varphi_2) = \mathbf{M}_{f,1}(\varphi_1) \cdot \mathbf{M}_{1,2'} \cdot \mathbf{M}_{2',2}(\varphi_2) \cdot \mathbf{M}_{2,3} \tag{5}$$

From the following relationship among the input shaft, planet wheel, and output shaft rotations:

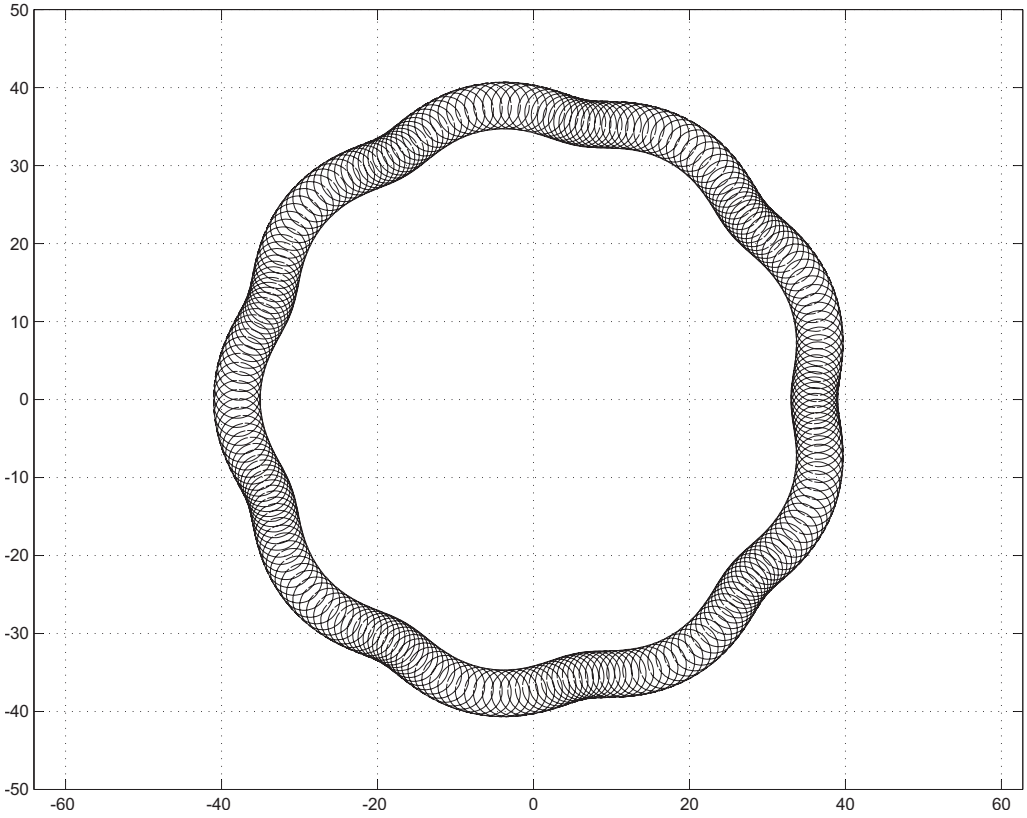

Fig. 5 The family of surfaces generated by a cylindrical roller and the profiles obtained from the two methods

$$\phi_2 = \varphi_1 + \varphi_2 \tag{6}$$

taking into account the definition of the reduction ratio itself $\tau = 1/n$ and the following relationship between the input shaft rotation (φ_1) and the output shaft rotation (ϕ_2):

$$\phi_2 = \varphi_1/n \tag{7}$$

the following relation between φ_1 and φ_2 can be obtained:

$$\varphi_2 = \varphi_1 \cdot \left(\frac{1}{n} - 1\right) \tag{8}$$

Having established a kinematical relationship between the input shaft and a generic cylindrical roller by means of the coordinate transformation matrix $\mathbf{M}_{f,3}(\varphi_1, \varphi_2(\varphi_1)) = \mathbf{M}_{f,3}(\varphi_1)$, it is now possible to determine the above mentioned family of surfaces.

The first step consists in defining the cylindrical roller profile and its unit normal vector equations in reference frame $\mathbf{S}_3$

$$\mathbf{r}_r^{(3)}(\theta) = \begin{bmatrix} R_r \cos\theta \\ R_r \sin\theta \\ 1 \end{bmatrix} \tag{9}$$

$$\mathbf{n}_r^{(3)}(\theta) = \begin{bmatrix} \cos\theta \\ \sin\theta \\ 0 \end{bmatrix} \tag{10}$$

The family of surfaces Σ_r (see Fig. 5) can be then derived projecting the cylindrical roller profile in the reference frame $\mathbf{S}_f$

$$\mathbf{r}_{\Sigma_r}^{(f)}(\varphi_1, \theta) = \mathbf{M}_{f,3}(\varphi_1) \cdot \mathbf{r}_r^{(3)} \tag{11}$$

In order to obtain the envelope of this family of surfaces, the equation of meshing

$$\left(\frac{\partial \mathbf{M}_{f,3}}{\partial \varphi_1} \cdot \mathbf{r}_r^{(3)}\right) \cdot (\mathbf{L}_{f,3} \cdot \mathbf{n}_r^{(3)}) = 0 \tag{12}$$

has to be solved with respect to θ as follows:

$$\theta = \tilde{\theta}(\varphi_1) \tag{13}$$

Since two envelopes exist at every instant (see Fig. 5), the equation of meshing provides two solutions, then particular attention has to be paid in choosing the right solution. The inner profile of the external ring gear is the solution of the system of equations composed by Eqs. (11) and (12) given by

$$\mathbf{r}_r^{(f)}(\varphi_1) = \mathbf{r}_{\Sigma_r}^{(f)}(\varphi_1, \tilde{\theta}(\varphi_1)) \tag{14}$$

In order to validate the above described procedure, the profile generated following this method has been compared with the profile determined adapting Blanche and Yang's method (see Ref. [3]) to the case of the external ring gear. In the following this method is briefly described.

The complex vector

$$\underline{A_P} = (R_b + R_g) \cdot e^{i\cdot\psi} + \rho \cdot e^{i\cdot(\psi+\delta)} = (R_b + R_g) \cdot e^{i\cdot\psi} - \rho \cdot e^{i\cdot\phi\cdot(1+R_b/R_g)} \tag{15}$$

where $\phi = \psi - 2\cdot\pi\cdot N/n$ with $N \in [1, n]$ describes the position of the center of the circle of radius R_r (see Fig. 3) rigidly connected to the generating circle with a distance between the centers equal to the eccentricity $|CO_g| = \rho$. The curve described by the vector $\underline{A_P}$ is an epitrochoid. The profile of the ring gear, computed as the envelope of all roller positions, is the curve described by the following complex vector (see Ref. [3] for details):

$$\underline{D_P} = R_b \cdot e^{i\cdot\psi} + (|AC| + R_r) \cdot e^{i\cdot(\psi-\gamma)} \tag{16}$$

where

Table 1 Sample data

Symbol	Value (mm)
R_b	33.3
R_g	3.7
R_r	3.0
ρ	1.0

$$|AC| = \sqrt{R_g^2 + \rho^2 - 2 \cdot \rho \cdot R_g \cos(\psi \cdot R_b/R_g)}$$

and

$$\tan(\gamma) = \frac{\rho \sin(\psi \cdot R_b/R_g)}{R_g - \rho \sin(\psi \cdot R_b/R_g)}$$

The profile of the external ring gear is a curve derived from an epitrochoid equidistant from the original curve by the radius R_r. Analytical and numerical investigations showed that the curve $\mathbf{r}_r^{(f)}(\varphi_1)$ is identical to this one. Figure 5 shows the overlapping profiles computed with the two methods and the family of surfaces generated by a cylindrical roller during its motion.

The main data of the sample cyclo-reducer are listed in Table 1.

3 Contact Forces Distribution

In this section a simplified method to calculate the forces acting on the parts of the reducer is presented. The study is performed under the following three assumptions:

1. perfect geometry
2. rigid bodies
3. negligible friction

Figure 6 shows the forces acting on the components of the reducer in a generic position, corresponding to a rotation $\varphi_{1,0}$ of the input shaft. This schema has been conceived on the basis of the following statements. At a given time, all the n cylindrical rollers and s output pins are in contact with the surface of the ring gear and the surfaces of the holes of the planet wheel, respectively. Nevertheless, only half of them take part in torque transmission, since only compressive forces can be transmitted by contacting surfaces. As a consequence, the cylindrical rollers transmit forces only when their angular position is among $\varphi_{1,0}$ and $\varphi_{1,0} + \pi$, and the output pins transmit forces only when their angular position is among $\varphi_{1,0} + \pi$ and $\varphi_{1,0} + 2 \cdot \pi$. In order to calculate these forces, the following equilibrium equations have been considered.

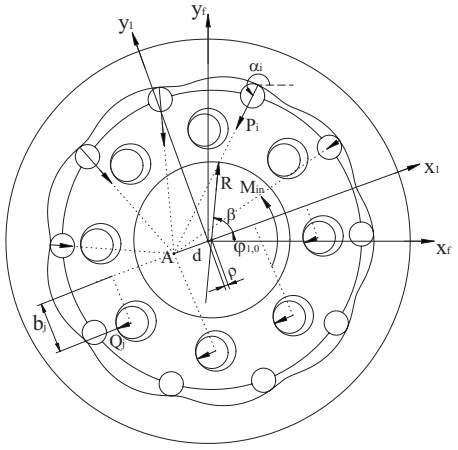

Fig. 6 Contact forces among cyclo-reducer elements

1. For the torque equilibrium of the input shaft,

$$M_{\text{in}} = R \cdot \rho \sin \beta \tag{17}$$

2. For the torque equilibrium of the output shaft,

$$M_{\text{out}} = \sum_{j=1}^{s} Q_j \cdot b_j \tag{18}$$

3. For the equilibrium of the planet wheel (i.e., equilibrium in the x_1 and y_1 directions and the torque equilibrium),

$$R \sin \beta - \sum_{i=1}^{n} |P_i \sin(\alpha_i - \varphi_{1,0})| = 0$$

$$R \cos \beta - \sum_{i=1}^{n} (P_i \cos(\alpha_i - \varphi_{1,0})) - \sum_{j=1}^{s} Q_j = 0 \tag{19}$$

$$(\rho + d) \cdot R \sin \beta = \sum_{j=1}^{s} Q_j \cdot b_j$$

Since the system is statically indetermined, the rigid body equilibrium equations (17)–(19) are insufficient to determine every force. In order to solve the problem without taking into account its elastic compliance, we have assumed that the modules of the forces P_i have a sinusoidal distribution between $\varphi_{1,0}$ and $\varphi_{1,0} + \pi$, and the modules of the forces Q_j are proportional to their arm b_j (see Refs. [4,2]). These considerations are expressed mathematically by the following equations:

$$|\mathbf{P}_i| \propto |\sin(\alpha_i - \varphi_{1,0})| \Rightarrow |\mathbf{P}_i| = P \cdot |\sin(\alpha_i - \varphi_{1,0})|$$
$$|\mathbf{Q}_j| \propto b_j \Rightarrow |\mathbf{Q}_j| = Q \cdot b_j \tag{20}$$

Introducing these assumptions into Eqs. (17)–(19), the following expressions of forces P_i, Q_j, and R can be derived:

$$P_i = \frac{M_{\text{in}} \cdot |\sin(\alpha_i - \varphi_{1,0})|}{\rho \cdot \sum_{i=1}^{n} \sin^2(\alpha_i - \varphi_{1,0})}$$

$$Q_j = M_{\text{in}} \cdot \left((1 + R_b/R_g) \cdot \frac{b_j}{\sum_{j=1}^{s} b_j^2} \right) \tag{21}$$

$$R = \frac{M_{\text{in}}}{\rho \sin \beta}$$

Observing the structure of these equations, it is possible to draw some considerations about the influence of the design parameters on the contact forces among the elements of the reducer. For instance, it is evident that as the eccentricity ρ increases, the forces P_i and R decrease. In the above-developed analysis, a reducer with only one planet wheel has been considered. Actually, in order to balance the forces acting on the case, the cycloidal reducer has two (or even more) planet wheels. The cycloidal reducer used for tests has a second planet wheel, with a phase difference of 180 deg with respect to the first. In the theoretical approach, we have assumed that the torque is equally shared by the two wheels. Figure 7 shows a typical result of the distribution of forces on rollers and pins with M_{in}=3 Nm.

4 Power Loss and Theoretical Mechanical Efficiency

In this section, a simplified procedure to determine the theoretical mechanical efficiency of the cycloid drive is presented. This procedure is developed in order to determine a parameter (the mechanical efficiency) that can be easily measured and then used to tune the analytical model. For simplicity, in the following we refer to the mechanical efficiency as the efficiency. Only the power losses listed below are considered, since a comparison with the experimental results showed that these are the major contribu-

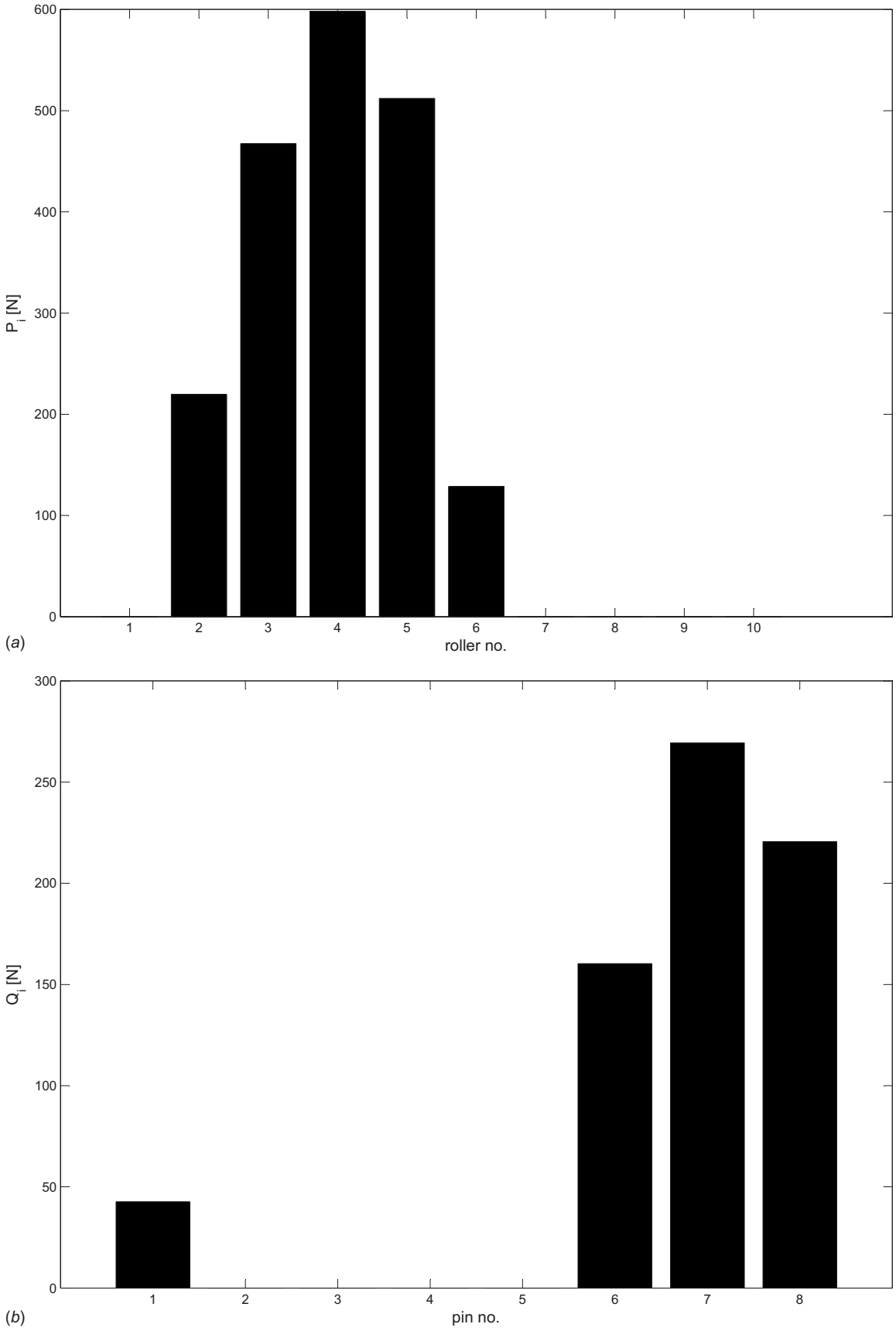

Fig. 7 Force distribution on rollers and pins for a 3 nm input torque

tions. The analytical expressions of each power loss are developed on the basis of the kinematical analysis and the simplified force computation previously developed.

4.1 Friction in the Bearing Between the Planet Wheel and the Input Shaft. The frictional torque of the bearing, as a first approximation, can be determined as

$$M_a = \mu \cdot R \cdot D/2 \tag{22}$$

Then, the power loss due to the bearing friction could be computed by means of the following equation:

$$W_{M_a} = M_a \cdot (\omega_{\text{inner}} - \omega_{\text{outer}}) \tag{23}$$

4.2 Friction Between the Pins of the Output Shaft and the Holes of the Planet Wheel. The kinematical analysis shows that a sliding contact between the pins of the output shaft and the holes of the planet wheel occurs. The consequent power loss for a single pin can be obtained by means of the following equation:

$$W_{Q_j} = \mathbf{F}_{Q_j} \cdot \mathbf{v}_{Q_j} \tag{24}$$

Since the previously developed kinematical analysis yields to the following expressions of the sliding velocity components in the reference frame $\mathbf{S}_f$ (see Fig. 6):

$$\begin{aligned} v_{Q_j x_f} &= \rho \sin\left(\varphi_{1,0} \cdot \frac{\tau - 1}{\tau}\right) \cdot \frac{\tau - 1}{\tau} \cdot \omega_{\text{in}} \\ v_{Q_j y_f} &= \rho \cos\left(\varphi_{1,0} \cdot \frac{\tau - 1}{\tau}\right) \cdot \frac{\tau - 1}{\tau} \cdot \omega_{\text{in}} \end{aligned} \tag{25}$$

This contribution to the power loss can be determined by means of the following equation:

$$W_Q = \sum_{j=1}^{s} f_{Q_j} \cdot Q_j \cdot v_{Q_j} \tag{26}$$

4.3 Friction Between the Cylindrical Rollers, the Surface of the Ring Gear, and Their Housing in the Planet Wheel. In the correct working condition, there is a rolling contact between the cylindrical rollers and the surface of the ring gear, and a sliding contact between the rollers and the planet wheel in the semicircular houses on its profile. The power loss due to the latter contact can be determined as [9]

$$W_{p_i} = R_r \sin(\arctan(f_{P_i})) \cdot |\mathbf{P}_i| \cdot |\omega_{P_i}| \tag{27}$$

The modulus of the relative rotational speed ω_{P_i} can be determined as the sum of the absolute rotational speed of the cylindrical roller

$$\begin{aligned} |\omega_{P_i}| = \frac{\omega_{\text{in}}}{\tau \cdot R_r} \cdot \Bigg[& (R_b + R_g)^2 + \tau^2 \cdot \rho^2 + \cdots \\ & - 2 \cdot \tau \cdot \rho \cdot (R_b + R_g) \cdot \sin\left(\left(1 - \frac{1}{\tau}\right) \cdot \varphi_{1,0}\right) \Bigg]^{1/2} \end{aligned} \tag{28}$$

and the absolute rotational speed of the planet wheel.

This contribution to the power loss can be determined by means of the following equation:

$$W_P = \sum_{i=1}^{n} W_{p_i} \tag{29}$$

4.4 Total Power Loss. The total power loss can then be computed as the sum of these contributions. It is possible to calculate the theoretical efficiency of the reducer as

$$\eta_{\text{theo}} = \frac{W_{\text{in}} - W_d}{W_{\text{in}}} = \frac{W_{\text{in}} - (W_{M_a} + W_Q + W_P)}{W_{\text{in}}} \tag{30}$$

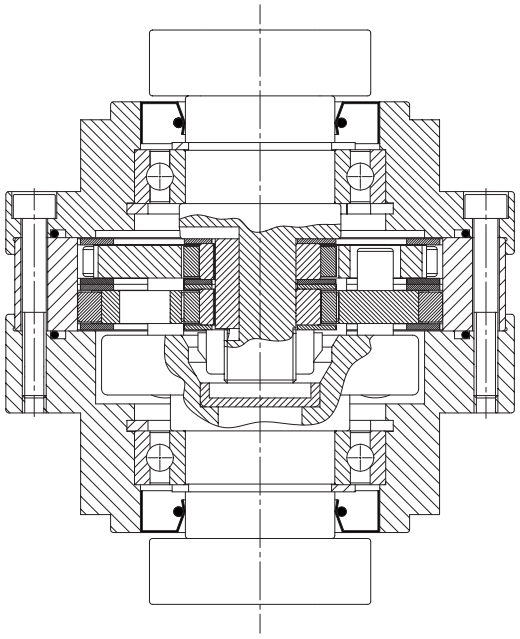

Fig. 8 Section view of the cycloidal speed reducer used in the tests

5 Experimental Tests

Several experimental tests have been performed to measure the efficiency of the cycloidal reducer in order to tune the analytical model. These tests have been performed on a rig composed by a dc electric motor, a torque meter to measure the input torque, the reducer under test (Fig. 8), a second torque meter to measure the output torque, and another dc electric motor acting as a brake. As shown in Fig. 9, the reducer has been mounted on the test rig with two universal joints on the input and output shafts in order to compensate for any misalignment between the reducer and shafts of the two electric motors. By means of several thermocouples, the temperature of the reducer has been continuously monitored.

The tests have been performed at different operating conditions, in order to appreciate the influence of speed and torque on the efficiency of the reducer. Every test has been performed at constant speed and torque, until the reducer reached the thermal regime, i.e., the reducer temperature became constant. Figure 10 shows the reducer temperature during the warm up phase of some tests. During tests, it has been noticed that the speed has a small influence on the efficiency and that at the steady thermal conditions the efficiency of the reducer increases with the torque, reaching values comparable with traditional cycloidal reducers [2]. Other solutions [10] can reach higher values of mechanical efficiency. Table 2 summarizes the efficiency measured (after the thermal equilibrium has been reached) in several operating conditions.

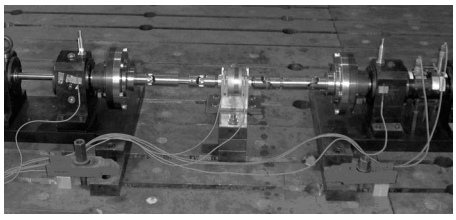

Fig. 9 Cycloidal reducer on the test rig

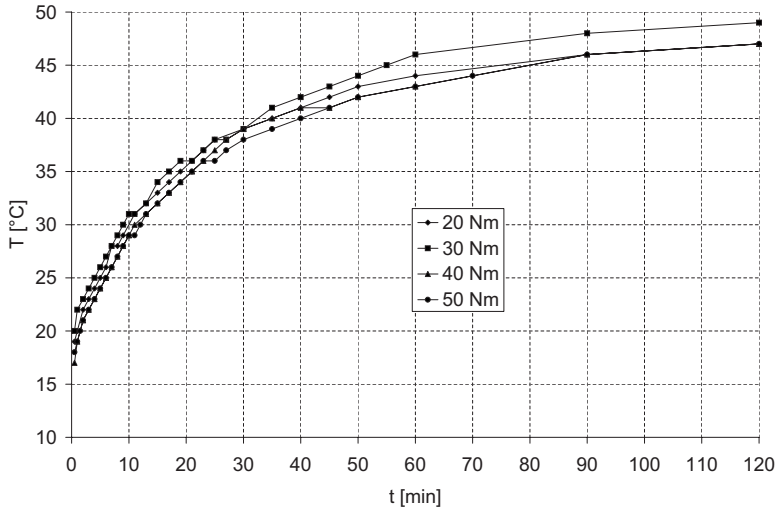

Fig. 10 Reducer temperature during tests at 500 rpm

6 Experimental and Theoretical Results Comparison

A tuning of the theoretical model has been performed on the basis of the experimental results. In particular, the friction coefficient is derived starting from the measured efficiency.

The theoretical efficiency is strongly dependent on the coefficients of friction μ, f_{P_i}, and f_{Q_j} used for the calculation: this means that a tuning process of the model must pass through the determination of their values. The bearing between the input shaft and the planet wheel is a full-complement cylindrical roller bearing, then, according to Ref. [11], μ can be assumed equal to 0.020. As a first approximation, we assume that f_{P_i} and f_{Q_j} have the same value f, that, at steady temperature conditions, depend on the torque because, as said before, the speed has a small influence. Since it would be very difficult to measure the friction coefficient, a quadratic relationship $f=f(M_{\text{in}})$ between the friction coefficient f and the input torque M_{in} has been developed using the results coming from the tests performed at 1000 rpm. In other words, the coefficients a, b, and c of the quadratic expression $f=a\cdot M_{\text{in}}^2+b\cdot M_{\text{in}}+c$ have been determined minimizing the difference between the experimental results at 1000 rpm and the theoretical results, including in the model of the above mentioned quadratic expression of the friction coefficient f. The theoretical efficiency of the reducer has then been calculated at all the other operating conditions. Table 2 shows the measured values of efficiency in comparison with the corresponding calculated ones and their difference. The computed values show a good agreement with the experimental results.

Table 2 Comparison between the experimental and theoretical results

Speed (rpm)	M_{in} (N m)	f (/)	η_{theo} (/)	η_{exp} (/)	Δ (%)
500	2.9	0.045	0.76	0.75	−1.3
500	3.9	0.033	0.81	0.78	−3.8
500	4.6	0.029	0.84	0.83	−1.2
500	5.4	0.026	0.85	0.88	3.4
1000	2.9	0.045	0.76	0.75[a]	−1.3
1000	3.7	0.035	0.80	0.81[a]	1.2
1000	4.6	0.029	0.84	0.83[a]	−1.2
1000	5.6	0.026	0.85	0.85[a]	0.0
1500	3.1	0.042	0.77	0.72	−6.9
1500	3.9	0.033	0.81	0.79	−2.5
1500	4.9	0.027	0.84	0.80	−5.0
1500	5.6	0.026	0.85	0.85	0.0
2000	3.2	0.041	0.77	0.71	−8.5
2000	4.0	0.033	0.82	0.81	−1.2
2000	4.7	0.028	0.84	0.85	1.2
2000	5.4	0.026	0.85	0.89	4.5

[a]Results used for the calibration of the model.

7 Conclusions

In this work a theoretical and experimental analysis of a cycloidal speed reducer has been performed. The profile of the ring gear has been derived by applying the theory of gearing, and a simplified procedure to calculate for the distribution of forces on cyclo-reducer elements has been presented.

A comparison between the results coming from a series of experimental tests and the calculated theoretical efficiency has been performed.

Nomenclature

R_b = radius of the base circle
R_g = radius of the generating circle
R_r = radius of the cylindrical roller
ρ = eccentricity
h = thickness of the cylindrical roller
n = number of cylindrical rollers
m = number of lobes of the inner surface of the ring gear profile, it is assumed to be equal to $n-1$, unless otherwise specified
s = number of cylindrical pins of the output shaft
$\mathbf{M}_{i,j}$ = homogeneous coordinate transformation matrix from system j to system i
$\mathbf{L}_{i,j}$ = matrix to perform a transformation of vector components from system j to system i, obtained by eliminating the last row and the last column of the corresponding matrix $\mathbf{M}_{i,j}$
φ_1 = input shaft rotation
φ_2 = planet wheel rotation
ϕ_2 = output shaft rotation
$\mathbf{r}_k^{(j)}$ = position vector of the k entity projected in reference frame $\mathbf{S}_j$
$\mathbf{n}_k^{(j)}$ = unit normal vector of the k entity projected in reference frame $\mathbf{S}_j$
N = index identifying the generic cylindrical roller
M_{in} = input torque
$\mathbf{R}$ = crank reaction

$\mathbf{P}_i$ = force between the generic cylindrical roller and the external ring gear

$\mathbf{Q}_j$ = force between the generic output pin and the corresponding hole of the planetary wheel

$\mathbf{F}_{Q_j}$ = tangential force due to the friction between the pins of the output shaft and the holes of the planet wheel

β = angle between force $\mathbf{R}$ and the abscissa axis x_1

α_i = angle between force $\mathbf{P}_i$ and the abscissa axis x_f

b_j = arm of the force $\mathbf{Q}_j$

d = distance between the center of the ring gear and the intersection point A of all lines of action of the forces $\mathbf{P}_i$

μ = bearing coefficient of friction

ω_{in} = input rotational speed

ω_{out} = output rotational speed

ω_{inner} = bearing inner race speed

ω_{outer} = bearing outer race speed

D = bearing inner diameter

τ = reduction ratio

f_{P_i} = friction coefficient between the cylindrical rollers and their houses in the planet wheel

f_{Q_j} = friction coefficient between the pins of the output shaft and the holes of the planet wheel

ω_{P_i} = relative rotational speed between the cylindrical rollers and the planet wheel

$\mathbf{v}_{Q_j}$ = sliding speed between the pins of the output shaft and the holes of the planet wheel

W_{in} = input power

W_{M_a} = bearing power loss

W_{Q_j} = power loss between the jth pin of the output shaft and the corresponding hole of the planet wheel

W_{P_i} = power loss between the ith cylindrical roller and the planet wheel

η = mechanical efficiency

References

[1] Litvin, F., and Feng, P., 1996, "Computerized Design and Generation of Cycloidal Gearigs," Mech. Mach. Theory, **31**(7), pp. 891–911.

[2] Malhotra, S. K., and Parameswaran, M. A., 1983, "Analysis of a Cycloid Speed Reducer," Mech. Mach. Theory, **18**(6), pp. 491–499.

[3] Blanche, J., and Yang, D., 1989, "Cycloid Drives With Machining Tolerances," ASME J. Mech., Transm., Autom. Des., **111**, pp. 337–344.

[4] Chmurawa, M., and Lokiec, A., 2001. "Distribution of Loads in Cycloidal Planetary Gear (Cyclo) Including Modification of Equidistant," Proceedings of the 16th European ADAMS User Conference 2001, November 14–15, Berchtesgaden, Germany.

[5] Yan, H., and Lai, T., 2002, "Geometry Design of an Elementary Planetary Gear Train With Cylindrical Tooth Profiles," Mech. Mach. Theory, **37**(8), pp. 757–767.

[6] Hwang, Y.-W., and Hsieh, C.-F., 2007, "Geometric Design Using Hypotrochoid and Nonundercutting Conditions for an Internal Cycloidal Gear," ASME J. Mech. Des., **129**, pp. 413–420.

[7] Litvin, F. L., 1989, "Theory of Gearing," NASA Technical Report No. RP-1212 and AVSCOM Report No. TR-88-C-035.

[8] Ltivin, F. L., 1994, *Gear Geometry and Applied Theory*, Prentice-Hall, Englewood Cliffs, NJ.

[9] Sesini, O., 1964, *Meccanica Applicata Alle Macchine*, Vols. 1–5, Casa Editrice Ambrosiana, Milano.

[10] Li, X., He, W., Li, L., and Schmidt, L. C., 2004, "A New Cycloid Drive With High-Load Capacity and High Efficiency," ASME J. Mech. Des., **126**, pp. 683–686.

[11] Niemann, G., Winter, H., and Höhn, B.-R., 2005, *Maschinen-Elemente*, Springer-Verlag, Berlin.